DALTON
FULL PAPER

Synthesis and structural characterisation of the mixed metal clusters $[Rh_2Pt_3(\mu\text{-}CO)_5(CO)_4(PPh_3)_3]$ and $[Rh_2Pt_2(\mu\text{-}CO)_3(CO)_4(PPh_3)_3]$; crystal structure of $[Rh_2Pt_3(\mu\text{-}CO)_5(CO)_4(PPh_3)_3]$ †

Fiodor M. Dolgushin,[a] Elena V. Grachova,[b] Brian T. Heaton,[c] Jonathan A. Iggo,*[c] Igor O. Koshevoy,[b] Ivan S. Podkorytov,[d] Daniel J. Smawfield,[c] Sergey P. Tunik,*[b] Robin Whyman[c] and Aleksandr I. Yanovskii*[a]

[a] *A.N. Nesmeyanov Institute of Organoelement Compounds, 28 Vavilov Street, Moscow, 117813, Russia*
[b] *St. Petersburg University, Department of Chemistry, Universitetskii pr., 2, St. Petersburg, 198904, Russia*
[c] *Department of Chemistry, University of Liverpool, PO Box 147, Liverpool, UK L69 7ZD*
[d] *S.V. Lebedev Central Synthetic Rubber Research Institute, Gapsalskaya 1, St. Petersburg, 198035, Russia*

Received 23rd November 1998, Accepted 22nd March 1999

Two novel mixed metal rhodium–platinum clusters have been synthesized by the reaction of $[Rh_4(CO)_{12}]$ with $[Pt(PPh_3)_3]$. The structure of $[Rh_2Pt_3(\mu\text{-}CO)_5(CO)_4(PPh_3)_3]$ **1** has been established by a single crystal X-ray diffraction study. The tetranuclear cluster $[Rh_2Pt_2(\mu\text{-}CO)_3(CO)_4(PPh_3)_3]$ **2** has been characterised by FAB mass spectrometry and shown by various multinuclear NMR techniques (^{13}C, ^{31}P, $\{^{31}P–^{31}P\}$ COSY and $\{^{13}C–^{103}Rh\}$ and $\{^{31}P–^{103}Rh\}$ heteronuclear multiple quantum coherence, HMQC) to adopt a butterfly type structure. The carbonyl migration pathways in **2** have been established by a combination of EXSY and 1-D variable temperature measurements; independent localised exchange about the hinge rhodium atoms and interchange of bridging and semi-bridging carbonyls on the Pt–Rh bonds occur.

The synthesis and chemistry of mixed metal clusters have attracted considerable attention in recent years. Unambiguous characterisation of such compounds has relied on crystal structure determinations both to discover the geometry of the metal core and also the ligand environment. Spectroscopic techniques such as IR and NMR have played a secondary role in characterisation, IR in distinguishing CO ligand types (terminal, semi-bridge, bridge) and NMR in determining the number of ligand sites and their occupancies, particularly for COs and for clusters containing phosphines. NMR Spectroscopy, *via* variable temperature measurements, has also allowed pathways for ligand (H and/or CO) and metal rearrangements to be elucidated. However, except for homo- and heterometallic rhodium containing clusters,[1] characterisation of the metal core by NMR spectroscopy has generally not been possible due to the low sensitivity and/or lack of a suitable spin of the metal nuclides.

We have previously reported the use of 1-D double resonance techniques to obtain and assign the metal core resonances in a series of phosphine-substituted hexanuclear rhodium carbonyl clusters using ^{31}P or ^{13}C as the detector nucleus.[2,3] More recently we have described the benefits and difficulties of using heteronuclear multiple quantum coherence (HMQC) NMR spectroscopy in the inverse mode to detect the metal nuclei in compounds of this type.[4] We have also reported the advantages of using NMR exchange spectroscopy (EXSY) to establish the exact pathway of the carbonyl fluxional process in these compounds and have shown that it varies with, and depends crucially on, the nature of the heteroligand.[5] In this paper we report the synthesis and structural characterisation of two new Rh–Pt clusters; $[Rh_2Pt_3(\mu\text{-}CO)_5(CO)_4(PPh_3)_3]$ **1** and $[Rh_2Pt_2(\mu\text{-}CO)_3(CO)_4(PPh_3)_3]$ **2**. Cluster **1** has been structurally characterised by X-ray diffraction and **2** has been characterised by various multinuclear NMR techniques (^{13}C, ^{31}P, $\{^{31}P–^{31}P\}$ COSY and $\{^{13}C–^{103}Rh\}$ and $\{^{31}P–^{103}Rh\}$ HMQC). Determination of the carbonyl migration pathways in **2** by a combination of EXSY and 1-D variable temperature measurements was crucial in the structural characterisation of **2**.

The preparation and behaviour of Rh–Pt compounds are of especial interest due to the well known catalytic properties of the individual metals in various organic reactions. Various Rh–Pt clusters, including anionic carbonyls[6–10] and neutral compounds[11–13] have been prepared and studied during the last fifteen years.

Results and discussion

The reaction between $[Rh_4(CO)_{12}]$ and $[Pt(PPh_3)_3]$ affords two new mixed metal Rh–Pt carbonyl–phosphine clusters, eqn. (1).

$$[Rh_4(CO)_{12}] + [Pt(PPh_3)_3] \longrightarrow \underset{\mathbf{1}}{[Rh_2Pt_3(CO)_9(PPh_3)_3]} + \underset{\mathbf{2}}{[Rh_2Pt_2(CO)_7(PPh_3)_3]} \quad (1)$$

The IR data for clusters **1** and **2** are given in Table 1.

Structural characterisation of $[Rh_2Pt_3(CO)_9(PPh_3)_3]$ 1

The molecular structure of cluster **1**, determined by X-ray diffraction, is shown in Fig. 1 and selected bond lengths and angles are given in Table 2. The five metal atoms of the Rh_2Pt_3-cluster core form a trigonal bipyramid (*TBPY*) with one platinum and two rhodium atoms in the equatorial plane of the polyhedron. The 72 electron cluster is electron precise according to Wade's

† *Supplementary data available*: calculated and experimental mass spectra. For direct electronic access see http://www.rsc.org/suppdata/dt/1999/1609/, otherwise available from BLDSC (No. SUP 57527, 4 pp.) or the RSC Library. See Instructions for Authors, 1999, Issue 1 (http://www.rsc.org/dalton).

Table 1 IR Spectroscopic data for the complexes

Complex	IR/cm^{-1}			
1 $[Rh_2Pt_3(\mu\text{-}CO)_5(CO)_4(PPh_3)_3]$ [a]	2026s	1994s	1894w	1842s
	1822s	1764m	1734w	
2 $[Rh_2Pt_2(\mu\text{-}CO)_3(CO)_4(PPh_3)_3]$ [b]	2042m	2022s	1990m	1873w
	1830 (sh)	1807s	1724w	

[a] Recorded in CH_2Cl_2. [b] Recorded in $CHCl_3$.

Table 2 Selected bond lengths (Å) and angles (°) for cluster **1**

Pt(1)–C(1)	1.89(2)	Pt(3)–C(6)	2.07(2)
Pt(1)–C(3)	2.03(1)	Pt(3)–P(3)	2.257(4)
Pt(1)–P(1)	2.283(4)	Pt(3)–Rh(4)	2.682(2)
Pt(1)–Rh(5)	2.858(1)	Pt(3)–Rh(5)	2.696(1)
Pt(1)–Rh(4)	2.945(2)	Rh(4)–C(7)	1.89(2)
Pt(1)–Pt(3)	3.011(1)	Rh(4)–C(4)	2.00(1)
Pt(2)–C(2)	1.87(2)	Rh(4)–C(9)	2.12(2)
Pt(2)–C(4)	2.07(2)	Rh(4)–C(5)	2.19(2)
Pt(2)–P(2)	2.264(4)	Rh(4)–Rh(5)	2.696(2)
Pt(2)–Rh(4)	2.773(1)	Rh(5)–C(8)	1.86(2)
Pt(2)–Rh(5)	2.924(1)	Rh(5)–C(3)	2.00(1)
Pt(2)–Pt(3)	2.992(1)	Rh(5)–C(6)	2.10(1)
Pt(3)–C(5)	2.07(2)	Rh(5)–C(9)	2.12(2)
Rh(5)–Pt(1)–Rh(4)	55.35(4)	Pt(3)–Rh(4)–Pt(1)	64.50(4)
Rh(5)–Pt(1))–Pt(3)	54.61(3)	Rh(5)–Rh(4)–Pt(1)	60.68(4)
Rh(4)–Pt(1)–Pt(3)	53.52(3)	Pt(2)–Rh(4)–Pt(1)	119.06(4)
Rh(4)–Pt(2)–Rh(5)	56.42(3)	Pt(3)–Rh(5)–Rh(4)	59.67(4)
Rh(4)–Pt(2)–Pt(3)	55.30(3)	Pt(3)–Rh(5)–Pt(1)	65.60(3)
Rh(5)–Pt(2)–Pt(3)	54.20(3)	Rh(4)–Rh(5)–Pt((1)	63.98(4)
Rh(4)–Pt(3)–Rh(5)	60.18(4)	Pt(3)–Rh(5)–Pt(2)	64.19(4)
Rh(4)–Pt(3)–Pt(2)	58.19(4)	Rh(4)–Rh(5)–Pt(2)	58.95(4)
Rh(5)–Pt(3)–Pt(2)	61.62(3)	Pt(1)–Rh(5)–Pt(2)	116.97(4)
Rh(4)–Pt(3)–Pt(1)	61.99(4)	Rh(5)–C(3)–Pt(1)	90.5(6)
Rh(5)–Pt(3)–Pt(1)	59.80(3)	Rh(4)–C(4)–Pt(2)	85.9(6)
Pt(2)–Pt(3)–Pt(1)	110.39(3)	Pt(3)–C(5)–Rh(4)	78.2(6)
Pt(3)–Rh(4)–Rh(5)	60.16(4)	Pt(3)–C(6)–Rh(5)	80.4(5)
Pt(3)–Rh(4)–Pt(2)	66.50(5)	Rh(5)–C(9)–Rh(4)	78.9(5)
Rh(5)–Rh(4)–Pt(2)	64.63(4)	P(3)–Pt(3)–Pt(1)	127.9(1)
Rh(5)–Pt(1)–P(1)	133.4(1)	P(3)–Pt(3)–Pt(2)	121.5(1)
Rh(5)–Pt(2)–P(2)	167.8(1)	P(1)–Pt(1)–Pt(3)	145.7(1)
Rh(4)–Pt(1)–P(1)	160.1(1)	P(2)–Pt(2)–Pt(3)	135.9(1)
Rh(4)–Pt(2)–P(2)	133.0(1)		
C(1)–Pt(1)–C(3)	170.7(1)		
C(2)–Pt(2)–C(4)	168.3(1)		

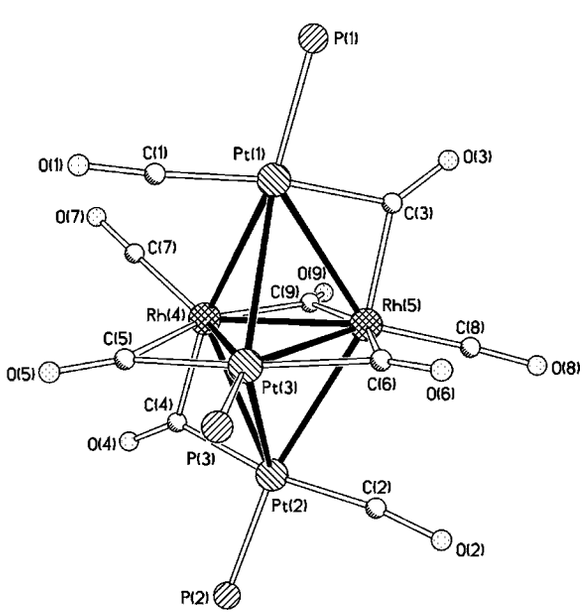

Fig. 1 Molecular structure of $[Rh_2Pt_3(\mu\text{-}CO)_5(CO)_4(PPh_3)_3]$ **1**.

rules.[14] This type of electron precise *TBPY* cluster has been found previously, *e.g.* $[Os_5(CO)_{16}]$ and its derivatives,[15,16] $[Fe_2Ir_3(CO)_{14}]^-$,[17] $[Ir_2Ru_3(CO)_{14}]^{2-}$,[18] $[ReIr_4(CO)_{12}(PPh_3)_2]^-$,[18] $[Rh_4Pt(CO)_{12}]^{2-}$,[7] and $[Ir_4Pt(CO)_{12}]^{2-}$,[20] but is relatively unusual compared to the "electron-excess" 76 electron, trigonal bipyramidal clusters such as $[Rh_4Pt(CO)_{14}]^{2-}$,[7] $[Rh_5(CO)_{15}]^-$,[21] *etc.*[22–31]

The structure of the $\{Rh_2Pt_3(\mu\text{-}CO)_5\}$ fragment of cluster **1** is very similar to the corresponding parts of $[Rh_5(\mu\text{-}CO)_5(CO)_{10}]^-$ [21] and $[Rh_5(\mu\text{-}CO)_6(CO)_8I]^{2-}$.[24] Metal–metal bond distances in the cluster core of **1** depend strongly on the nature of the interacting metal atoms and, as in the pentarhodium analogues, on whether this interaction is equatorial–equatorial (eq–eq) or equatorial–axial (eq–ax). Each edge of the equatorial plane in the trigonal bipyramid is spanned by a bridging carbonyl and the Rh–Rh distance [2.696(2) Å] is close to the average analogous distances found in $[Rh_5(\mu\text{-}CO)_5(CO)_{10}]^-$ (2.734 Å) and $[Rh_5(\mu\text{-}CO)_6(CO)_8I]^{2-}$ (2.715 Å). Interestingly the two equatorial Rh–Pt distances in **1** are slightly shorter, Pt(3)–Rh(4) 2.682(2) and Pt(3)–Rh(5) 2.696(1) Å, than the analogous Rh–Rh bond distance, despite the presence of the larger Pt atom. The eq–ax metal–metal distances in **1** are considerably longer than the eq–eq distances; the CO-bridged eq–ax Rh–Pt distances are Pt(1)–Rh(5) 2.858(1) and Pt(2)–Rh(4) 2.773(1) Å with the non-bridged edges being significantly longer, Pt(1)–Rh(4) 2.945(2) and Pt(2)–Rh(5) 2.924(1) Å. This difference in eq–eq and eq–ax bond lengths is typical for *TBPY* polyhedra and was found for both the Rh_5 clusters mentioned above.[21,24] The Pt–Pt distances, Pt(1)–Pt(3) 3.011(1) and Pt(2)–Pt(3) 2.992(1) Å, are the longest in the metal core of **1** as might reasonably be expected.

The carbonyl arrangement in cluster **1** consists of four terminal and five bridging CO ligands. Of the four terminal carbonyls, one is associated with each of the equatorial rhodium atoms and one with each of the apical platinum atoms. Bond lengths for the terminal M–C–O fragments are given in Table 2 and are typical for this type of cluster.

It is worthwhile to compare briefly the structure of cluster **1** with other known trigonal bypyramidal clusters which have been discussed recently.[19] The co-ordination geometry of the ligands around both apical Pt is T-shaped and, in both cases, the PPh_3 is almost *trans* to the non-CO-bridged Pt–Rh edge rather than the Pt–Pt edge (see Table 2). This can be compared with the structure of $[Rh_5(CO)_{14}(PPh_3)]^-$ [30] which contains an approximately square pyramidal $\{Rh(CO)_2(PPh_3)(\mu\text{-}CO)_2\}$ group with PPh_3 *trans* to the only non-bridged Rh_{ap}–Rh_{eq} edge rather than a CO-bridged edge. This follows the preference for PR_3 to occupy sites *trans* to non-bridged metal–metal vectors in di-, tri-, tetra-, penta- and hexa-nuclear clusters noted previously.[32]

Structural characterisation of $[Rh_2Pt_2(CO)_7(PPh_3)_3]$ 2

Suitable crystals of cluster **2** for an X-ray diffraction crystal structure determination could not be obtained; the structure proposed below has been elucidated on the basis of FAB-mass spectrometric and multinuclear NMR spectroscopic data and by comparison with the structurally characterised, analogous iridium and cobalt compounds $[Pt_2Ir_2(CO)_7(PPh_3)_3]$ [33] **3**, $[Pt_2Co_2(CO)_8(PPh_3)_2]$ [34] **4**, and $[Pt_2Co_2(CO)_8(COD)]$ [35] **5**, the structures of which are shown schematically below, and with $[Pt_2Os_2H_2(CO)_8\{P(C_6H_{11})_3\}_2]$ [36] **6**.

The FAB mass spectrum of cluster **2** shows a molecular ion at $m/z = 1578$. Several fragmentation ions are also seen; the main series (from $m/z = 1578$ to 1382) corresponds to the sequential loss of seven CO ligands. The isotopic distribution pattern expected for the ion $[Rh_2Pt_2(PPh_3)_3]^+$ has been calculated and matches well with the observed isotopic pattern of the fragment ion at $m/z = 1382$ (see SUP 57527). These data confirm the presence of two Pt atoms in the metal core of **2** and indicate that the probable molecular formula is $[Rh_2Pt_2(CO)_7(PPh_3)_3]$.

The clusters **2**–**6** are electron deficient (according to the usual electron counting rules) by two electrons per platinum atom,

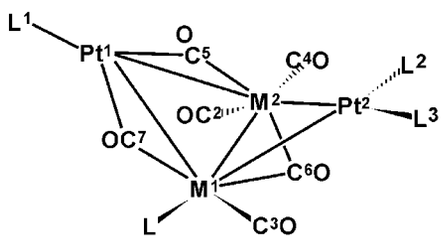

	M	L	L^1	L^2	L^3
2	Rh	Ph_3P^3	Ph_3P^1	Ph_3P^2	C^1O
3	Ir	Ph_3P	Ph_3P	Ph_3P	CO
4	Co	CO	Ph_3P	Ph_3P	CO
5	Co	CO	CO	COD	

having only 58 cluster core electrons, and adopt semi-closed tetrahedral/butterfly cores; it is reasonable to suppose that $[Pt_2Rh_2(CO)_7(PPh_3)_3]$ will adopt a similar structure. The Pt–Pt distances in **3**, **4**, **5** and **6** are fairly long (2.976, 2.987, 2.9546 and 3.206 Å respectively) indicative of at most weak Pt–Pt bonding.

The $\{^{31}P–^{103}Rh\}$ and $\{^{13}C–^{103}Rh\}$ heteronuclear multiple quantum coherence NMR spectra of cluster **2** have been obtained and show correlations at $\delta_{Rh} = -227$, Rh(1), and -206, Rh(2), respectively indicating the presence of two different rhodium sites in the molecule; Rh(1) is thus attached to triphenylphosphine whereas Rh(2) is attached to a terminal carbonyl ligand. The reasons for the lack of a correlation in the μ-CO region of the $\{^{13}C–^{103}Rh\}$ HMQC NMR spectrum of **2** are complex and will be discussed fully elsewhere.[4] Briefly, coupling of the bridging carbonyl to two rhodium spins results in the HMQC spectrum being distorted by transitions in which both rhodium spins 'flip'. This results both in sensitivity distortions (in extreme cases the single quantum cross peak intensity is zero!) and/or in the appearance of additional cross-peaks displaced from the rhodium chemical shift. These effects are not refocussed by the HMQC pulse sequence. In the present case the situation is further complicated by the extreme fluxionality of the cluster. The line widths in the 1-D spectrum are of the order of the rhodium–carbon couplings; the ^{13}C multiplets are barely resolved. As a result, there is fast decay of the magnetisation during the HMQC pulse sequence.

The limiting low temperature ^{31}P NMR spectrum of cluster **2**, Fig. 2(b), consists of three multiplets of 1:1:1 relative intensity in agreement with the cluster composition found in the FAB mass spectrum. Two of these signals, centred at δ 39.5 and 20.5, display one bond Pt–P coupling, $^1J_{PtP} = 4775$ and 3480 Hz respectively, and can be assigned to phosphorus ligands P(1) and P(2) respectively, bound to Pt(1) and Pt(2) respectively. The resonance of P(1) also shows a long range platinum–phosphorus coupling, $J_{Pt(2)P} = 300$ Hz. An additional coupling on the resonance of P(2) has been shown by $^{31}P–^{31}P$ COSY to be due to a long range three bond phosphorus–phosphorus coupling, $^3J_{PP} = 127$ Hz, to the third phosphorus nucleus, P(3). Atom P(3) gives a second order multiplet centred at δ 27.5 due to a one bond interaction with rhodium, $^1J_{RhP}$ *ca.* 125 Hz, a two bond interaction with Pt(2), $^2J_{PtP}$ *ca.* 127 Hz, and the three bond coupling with P(2) mentioned above. It is assigned to the phosphorus atom bound to Rh(1). The limiting low temperature ^{31}P NMR spectrum of **2** has been simulated based on this assignment and is shown in Fig. 2(a).

We have previously discussed the influence of stereochemistry on the magnitude of two and three bond couplings in phosphine substituted derivatives of the octahedral $[Rh_6(CO)_{16}]$ cluster.[2] Extrapolation of these results to cluster **2** allows the elucidation of the essential co-ordination environment of the phosphorus ligands. The presence of a three bond P–P coupling in the low temperature ^{31}P NMR spectrum fixes the relative

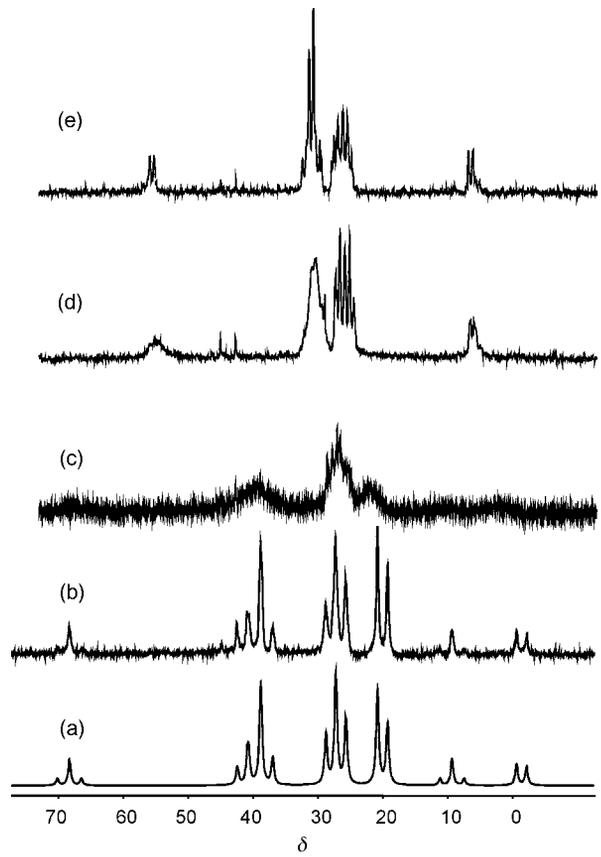

Fig. 2 Variable temperature ^{31}P NMR spectra of cluster **2**: (a) simulated spectrum, 158 K, (b) experimental spectrum, 158 K, (c) 205 K, (d) 250 K, (e) 298 K.

positions of P(2) and P(3) in a *trans-trans* conformation across the Pt(2)–Rh(1) bond whilst the absence of this coupling between P(1) and P(2) requires that these phosphorus nuclei are either *cis-cis* or *cis-trans.* Similarly, two bond Pt(2)–P(3) coupling points to a *trans* disposition of these atoms about the intervening rhodium nucleus. The ^{31}P NMR spectrum of **2** is thus entirely consistent with the structure of **2** being analogous to those of **3**–**5** ($M^1 = M^2 = Rh$; $L = L^1 = L^2 = PPh_3$, $L^3 = CO$) with the disposition of the phosphine ligands being unambiguously determined by the various couplings observed.

The low temperature ^{13}C NMR spectrum of cluster **2** shows six resonances in the carbonyl region of relative intensities 1:2:1:1:1:1, Fig. 3(a). The resonance at δ 252.2, C(7)O, shows one bond coupling to both rhodium, $^1J_{RhC}$ 25 Hz, and platinum, $^1J_{PtC}$ 835 Hz, and can be assigned to a carbonyl ligand bridging a rhodium–platinum bond. The resonance(s) of intensity two, centred around δ 244, results from accidental overlap of the resonances of two carbonyl ligands, C(5)O and C(6)O, which bridge Pt–Rh (δ_C 244.5, $^1J_{PtC} = 1003$ and $^1J_{RhC} = 23$ Hz) and Rh(1)–Rh(2) (δ_C 244.4, $^1J_{RhC} = 23$ Hz) edges respectively. This assignment accounts for the intensities of the platinum satellites (1/8) and the poorly resolved triplet structure of the central line of C(6)O. Although chemical shift and coupling data do not allow unambiguous assignment of C(7)O and C(5)O, EXSY data (see below) allow the assignment shown to be made.

The highest field resonance, δ_C 186.9, is readily assigned to C(1)O, a terminal carbonyl ligand on platinum, on the basis of a one bond Pt–C coupling constant of 1652 Hz. Similarly, the resonance centred at δ 191.7 can be assigned to C(2)O, a terminal carbonyl on rhodium, $^1J_{RhC}$ 65 Hz. The HMQC $\{^{13}C–^{103}Rh\}$ NMR spectrum, Fig. 4, confirms that this carbonyl group is bound to Rh(2). The remaining two resonances, δ_C 201.4, C(3)O, and 196.6, C(4)O, are poorly resolved multiplets; the resolved couplings are 55 and 71 Hz respectively and fall

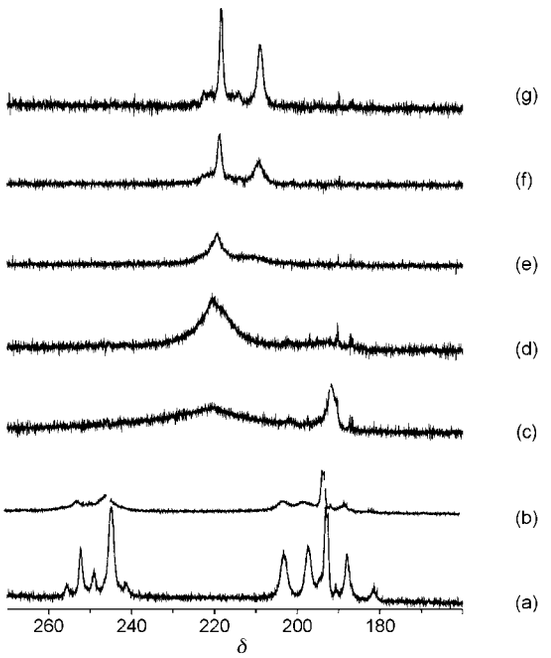

Fig. 3 Variable temperature ^{13}C NMR spectra of cluster **2**: (a) 180, (b) 190, (c) 220, (d) 240, (e) 260, (f) 280, (g) 300 K.

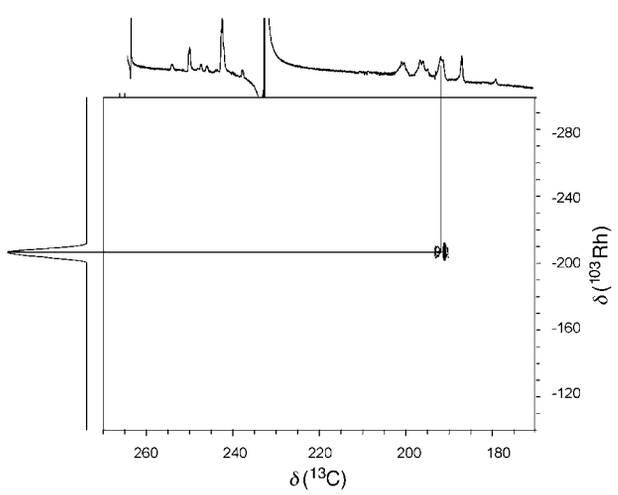

Fig. 4 ^{13}C-{^{103}Rh} HMQC NMR spectrum of cluster **2**.

in the range typical of one bond Rh–C couplings although no ^{103}Rh–^{13}C correlations were seen in the HMQC spectra for these resonances due to the extreme fluxionality of the cluster. The smaller couplings are only poorly resolved due to the extreme fluxionality of the cluster and might be due to weak interactions with either platinum or phosphorus or both. The EXSY data (see below) allow these resonances to be assigned to the carbonyl ligands on Rh(1) and Rh(2) respectively, possibly with a semi-bridging interaction with Pt(2).

Fluxional processes in cluster 2

The proposed structure of cluster **2** is asymmetric. Phosphorus-31 and ^{13}C NMR spectroscopy showed that **2** is stereochemically non-rigid above 158 K, the two enantiomers [see Scheme 1(a) and (c)] interconverting rapidly. The limiting low temperature ^{31}P and ^{13}C NMR spectra are shown in Figs. 2(b) and 3(a) respectively.

The variable temperature ^{31}P NMR spectra show that, at room temperature, the separate resonances of the phosphorus ligands on platinum collapse to a multiplet centred at δ 32.3 with $^{1}J_{PtP} = 4170$ Hz, $J_{Pt(remote)P} = 170$ Hz and $^{3}J_{PP} = 60$ Hz, *i.e.* essentially the averages of the respective values obtained from the low temperature spectrum. The fact that the platinum–

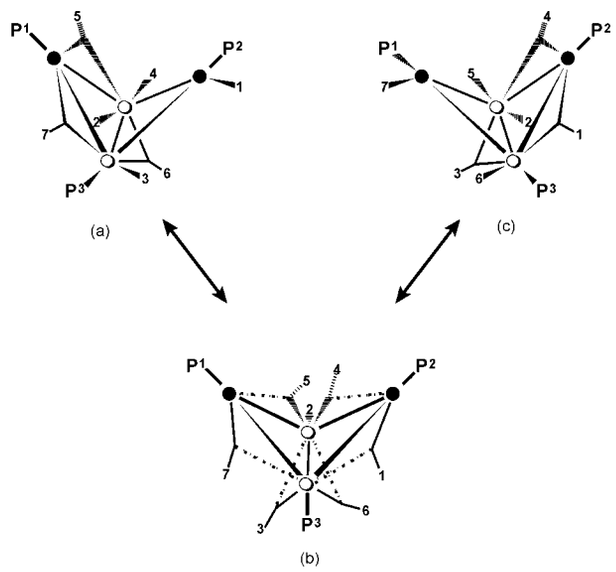

Scheme 1 The fluxional processes in cluster **2**; ● = Pt, ○ = Rh.

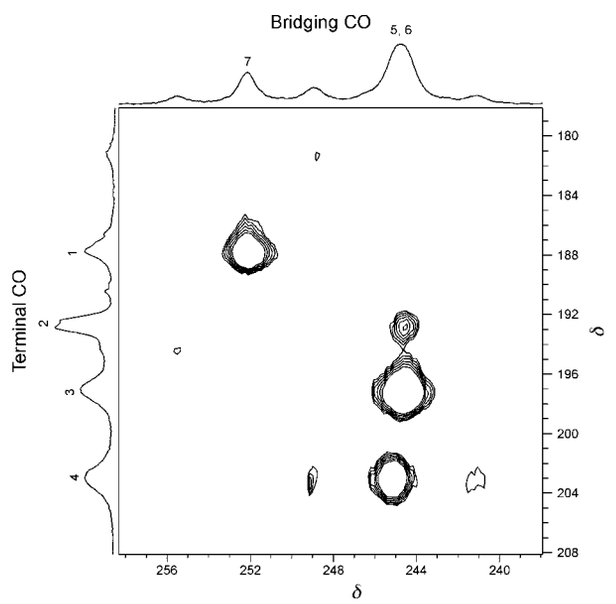

Fig. 5 The ^{13}C 2-D EXSY spectrum of cluster **2** in CD_2Cl_2 at 180 K, 50 ms mixing time. The area containing non-diagonal elements of the spectrum only is shown for the sake of simplicity.

phosphorus couplings result in doublet, rather than triplet, patterns implies that the phosphorus ligands are not exchanged between the platinum centres but that P(1) and P(2) are equivalenced by a pseudo exchange process, *i.e.* each phosphorus ligand remains bound to "its own" platinum centre rather than being exchanged between the two platinum atoms.

The resonance of the phosphorus ligand bound to rhodium appears as a complex multiplet since the fluxional process means that P(3) can be viewed as occupying alternately a position *trans* to P(1) then *trans* to P(2) thus introducing another coupling partner, P(1), for P(3). Unfortunately, the quality of the data obtained has not allowed simulation of the spectrum. We estimate $^{1}J_{Rh(1)P(3)} = 126$, $^{2}J_{PtP(3)} = 28$ and 10 and $^{3}J_{PP} = 58$ Hz.

The carbonyl exchange processes are revealed by the ^{13}C EXSY NMR spectrum of cluster **2** at 180 K, Fig. 5. Cross-peaks corresponding to exchange between C(3) and C(6) can be assigned to a localised oscillation about Rh(1) involving P(3), C(6) and C(3) and provides a pathway for the interchange of structures in which a CO ligand bridging the hinge of the butterfly occupies a position underneath the Pt(2) wingtip or under the Pt(1) wingtip and to move P(3) from a position

trans to Pt(2) to *trans* to Pt(1). The cross-peaks joining C(7) with C(1) and C(5) with C(4) are assigned to rearrangement of the bridging/semi-bridging CO framework from the Pt(1)-Rh(1)Rh(2) face to the Pt(2)Rh(1)Rh(2) face of the metal framework. This fluxional process reasonably requires C(4)O and C(5)O to be associated with the same rhodium, confirming the assignment of the ^{13}CO NMR spectrum given above. No cross-peaks are seen linking the two sets of localised exchanges, both localised processes, however, together are required in order to equivalence the butterfly wingtips.

At longer mixing times a further localised exchange about the rhodium hinge occurs: a cross-peak relating C(2)O and C(6)O is seen and at higher temperatures the ^{13}C NMR spectrum consists of only two resonances centred at δ 219 and 210 with relative intensity 4 : 3 respectively. The chemical shifts of these resonances correspond reasonably well with the weighted average positions of C(1), C(4), C(5) and C(7) (δ 221) and C(2), C(3) and C(6) (δ 212) allowing for the significant difference in temperatures, 180 and 300 K, and the associated temperature effect on the chemical shifts. The relative rates of the rotations about Rh(1) and Rh(2) are believed to reflect the influence of the phosphine ligand on Rh(1).[5]

Experimental

Reagents and solvents

The compounds $[Rh_4(CO)_{12}]$[37] and $Pt(PPh_3)_3$[38] were synthesized according to literature procedures. All solvents were dried over appropriate reagents and distilled prior to use. Reactions were carried out under dry argon. Products were separated in air by column chromatography on silica (5–40 mesh). The ^{31}P and ^{13}C NMR spectra were recorded on Bruker AM-500, AMX400 and AMX200 spectrometers; $[Cr(acac)_3]$ was added as a relaxation agent in the case of ^{13}C spectra. HMQC Experiments were run on a Bruker AMX200 instrument equipped with a three channel interface using an "in house" built probe. The IR spectra were recorded on a Specord M80 spectrometer.

Reaction of $[Rh_4(CO)_{12}]$ with $[Pt(PPh_3)_3]$

Depending on the solvent used to carry out the reaction, different compositions of reaction products were obtained. Chloroform was used to optimise the yields of **1**, whereas tetrahydrofuran gives the highest yields of **2**.

$[Rh_2Pt_3(\mu\text{-}CO)_5(CO)_4(PPh_3)_3]$ 1. A solution of $[Rh_4(CO)_{12}]$ (55 mg, 0.073 mmol) in chloroform (3 cm^3) was added to solid $[Pt(PPh_3)_3]$ (180.3 mg, 0.184 mmol) with stirring. Complete dissolution of the platinum complex required a few (<5) minutes. The reaction mixture was then diluted with heptane (1 cm^3), concentrated by rotary evaporation and transferred to a silica column (5–40 mesh, 2.5 × 8 cm). Chromatographic separation with hexane–chloroform mixtures gave the following bands in order of elution: hexane–chloroform 1 : 1.5, wide red band of **2** (43 mg), pink band containing trace amounts of unknown compound; hexane–chloroform 1 : 3, red band of **1** (12.3 mg), yellow band containing $[Rh(CO)_2(PPh_3)Cl]$ (26.7 mg). Single crystals of **1** were grown from heptane–chloroform solution at 263 K (Found: C, 39.3; H, 3.6. $C_{64}H_{46}Cl_3O_9P_3Pt_3Rh_2$ requires C, 39.4; H, 2.4%).

$[Rh_2Pt_2(\mu\text{-}CO)_3(CO)_4(PPh_3)_3]$ 2. A solution of $[Rh_4(CO)_{12}]$ (70.1 mg, 0.094 mmol) in tetrahydrofuran (5 cm^3) was added to solid $[Pt(PPh_3)_3]$ (226.3 mg, 0.231 mmol). Complete dissolution of the platinum complex required a few (<5) minutes. The solvent was then removed by rotary evaporation. The residue was dissolved in CH_2Cl_2 (2 cm^3), diluted with hexane (1.5 cm^3) and transferred to a silica column (5–40 mesh, 2.5 × 7 cm). Chromatographic separation with hexane–chloroform mixtures gave the following bands in order of elution: hexane–chloroform 1 : 1.5, wide red band containing **2** (149 mg); hexane–chloroform 1 : 3, narrow black band containing unidentified compound (10.6 mg) and trace amounts of **1** (Found: C, 45.3; H, 3.6. $C_{61}H_{45}O_7P_3Pt_2Rh_2$ requires C, 46.4; H, 2.9%).

Crystal structure determination of complex $1\cdot CHCl_3$

Crystal data and data collection parameters. $C_{64}H_{46}Cl_3O_9P_3Pt_3Rh_2$, $M = 1949.36$, monoclinic, space group $C2/c$ (no. 15), $a = 34.120(12)$, $b = 24.245(7)$, $c = 24.169(8)$ Å, $\beta = 134.21(2)°$, $V = 14331(8)$ Å^3 (by least-squares refinement of 24 carefully centred reflections in the $22 < 2\theta < 24°$ range), $T = 143$ K, graphite monochromated Mo-Kα radiation, $\lambda = 0.71073$ Å, $Z = 8$, $D_c = 1.807$ mg m^{-3}, $F(000) = 7376$, yellow prism with dimensions $0.4 \times 0.3 \times 0.2$ mm, μ(Mo-Kα) = 6.515 mm^{-1}. Absorption correction applied by the DIFABS method,[39] transmission factors 0.844–1.242; Siemens P3/PC diffractometer with LT-2 low-temperature attachment, θ–2θ scans, data collection range $4 < 2\theta < 50°$, $\pm h$, $+k$, $+l$, two standard reflections monitored every 98 showed no significant variation in intensity; 11927 independent reflections measured and used in the calculations.

Structure solution and refinement. The structure was solved by direct methods and subsequent Fourier-difference maps, and refined anisotropically by full-matrix least squares on F^2. The chloroform molecule of crystallisation was identified in the Fourier-difference series and refined in the anisotropic approximation. All H atoms were placed in geometrically calculated positions and included in the refinement using the riding model approximation with the $U_{iso}(H) = 1.2U_{eq}(C)$. The final $wR(F^2)$ was 0.1684 (on F^2 for 11877 reflections), with conventional $R1 = 0.0621$ [on F for 7441 reflections with $I > 2\sigma(I)$], for 757 parameters, goodness of fit = 0.96. All calculations were performed on an IBM PC using the SHELXTL PLUS 5 programs.[40]

CCDC reference number 186/1400.

See http://www.rsc.org/suppdata/dt/1999/1609/ for crystallographic files in .cif format.

Acknowledgements

We thank EPSRC for financial support and a studentship (to D. J. S.), the EC for financial support (INTAS - RFBR Grant No. 95-IN-RU-242) and B. T. H. thanks the Leverhulme Foundation for a Research Fellowship.

References

1 B. T. Heaton, J. A. Iggo, I. S. Podkorytov, D. J. Smawfield and S. P. Tunik, *Metal Clusters in Chemistry*, eds. P. Braunstein, L. Oro and P. Raithby, Wiley-VCH, Weinheim, to be published and refs. therein.

2 S. P. Tunik, I. S. Podkorytov, B. T. Heaton, J. A. Iggo and J. V. Sampanthar, *J. Organomet. Chem.*, 1998, **550**, 222.

3 C. Allevi, S. Bordoni, C. P. Clavering, B. T. Heaton, J. A. Iggo, C. Seregni and L. Garlaschelli, *Organometallics*, 1989, **8**, 385.

4 B. T. Heaton, J. A. Iggo, I. S. Podkorytov, D. J. Smawfield, S. P. Tunik and R. Whyman, *Chem. Commun.*, submitted for publication.

5 E. V. Grachova, B. T. Heaton, J. A. Iggo, I. Podkorytov, D. J. Smawfield, S. P. Tunik and R. Whyman, unpublished work.

6 A. Fumagalli, S. Martinengo, P. Chini, A. Albinati, S. Bruckner and B. T. Heaton, *J. Chem. Soc., Chem. Commun.*, 1978, 195.

7 A. Fumagalli, S. Martinengo, P. Chini, D. Galli, B. T. Heaton and R. D. Pergola, *Inorg. Chem.*, 1984, **23**, 7648.

8 A. Fumagalli, S. Martinengo and G. Ciani, *J. Organomet. Chem.*, 1984, **273**, C46.

9 A. Fumagalli, S. Martinengo, G. Ciani and A. Marturano, *Inorg. Chem.*, 1986, **25**, 592.

10 A. Fumagalli, S. Martinengo, D. Galli, A. Albinati and F. Ganazzoli, *Inorg. Chem.*, 1989, **18**, 2476.

11 M. Green, R. M. Mills, G. N. Pain, F. G. A. Stone and P. Woodward, *J. Chem. Soc.*, *Dalton Trans.*, 1982, 1309.
12 M. Green, J. A. K. Howard, G. N. Pain and F. G. A. Stone, *J. Chem. Soc.*, *Dalton Trans.*, 1982, 1327.
13 R. S. Dickson, G. D. Fallon, K. D. Hezle and M. J. Liddel, *J. Organomet. Chem.*, 1992, **430**, 221.
14 K. Wade, *Adv. Inorg. Chem. Radiochem.*, 1976, **18**, 1.
15 C. R. Eady, B. F. G. Johnson, J. Lewis, B. E. Reichert and G. M. Sheldrick, *J. Chem. Soc.*, *Chem. Commun.*, 1976, 271.
16 W. Weibin, R. J. Batchelor, W. B. F. Einstein, C.-Y. Lu and R. K. Pomeroy, *Organometallics*, 1993, **12**, 3598.
17 R. D. Pergola, L. Garlaschelli, F. Demartin, M. Manassero, N. Masciocchi, M. Sansoni and A. Fumagalli, *J. Chem. Soc.*, *Dalton Trans.*, 1989, 1109.
18 A. Sironi *et. al.*, unpublished results quoted in ref. 19.
19 P. Macchi, D. M. Proserpio and A. Sironi, *Organometallics*, 1997, **16**, 2101.
20 A. Fumagalli, R. D. Pergola, F. Bonacina, L. Garlaschelli, M. Moret and A. Sironi, *J. Am. Chem. Soc.*, 1989, **111**, 165.
21 A. Fumagalli, T. F. Koetzle, F. Takusagawa, P. Chini, S. Martinengo and B. T. Heaton, *J. Am. Chem. Soc.*, 1980, **102**, 1740.
22 G. Longoni, P. Chini, D. Lower and L. F. Dahl, *J. Am. Chem. Soc.*, 1975, **97**, 5034.
23 J. K. Ruff, R. P. White and L. F. Dahl, *J. Am. Chem. Soc.*, 1971, **93**, 2159.
24 S. Martinengo, G. Ciani and A. Sironi, *J. Chem. Soc.*, *Chem. Commun.*, 1979, 1059.
25 A. Fumagalli, L. Garlaschelli and R. D. Pergola, *J. Organomet. Chem.*, 1989, **362**, 197.
26 A. Ceriotti, G. Longoni, M. Manassero, M. Sansoni, R. D. Pergola, B. T. Heaton and D. O. Smith, *J. Chem. Soc.*, *Chem. Commun.*, 1982, 886; A. Ceriotti, G. Longoni, R. D. Pergola, B. T. Heaton and D. O. Smith, *J. Chem. Soc.*, *Dalton Trans.*, 1983, 1433.
27 A. Fumagalli, T. F. Koetzle and F. Takusagawa, *J. Organomet. Chem.*, 1981, **213**, 365.
28 A. Fumagalli, T. F. Koetzle, F. Takusagawa, P. Chini, S. Martinengo, B. T. Heaton and G. Longoni, *Am. Cryst. Assoc.*, *Ser. 2*, 1980, **7**, 16.
29 A. Fumagalli and G. Ciani, *J. Organomet. Chem.*, 1984, **272**, 91.
30 A. Fumagalli, S. Martinengo, D. Galli, C. Allevi, G. Ciani and A. Sironi, *Inorg. Chem.*, 1990, **29**, 1408.
31 F. Ragaini, F. Porta, A. Fumagalli and F. De Martin, *Organometallics*, 1991, **10**, 3785.
32 B. T. Heaton, *ACS Symp. Ser.*, 1983, **211**, 227.
33 S. Bhaduri, K. R. Sharma, W. Clegg, G. M. Sheldrick and D. Stalke, *J. Chem. Soc.*, *Dalton Trans.*, 1984, 2851.
34 P. Braunstein, J. Dehand and J. F Nenning, *J. Organomet. Chem.*, 1975, **92**, 117.
35 R. D. Adams, G. Chen, W. Wu and J. Yin, *Inorg. Chem.*, 1990, **29**, 4208.
36 L. J. Farrugia, J. A. K. Howard, P. Mitroprachachon and F. G. A. Stone, *J. Chem. Soc.*, *Dalton Trans.*, 1981, 1274.
37 S. Martinengo, G. Giordano and P. Chini, *Inorg. Synth.*, 1980, **20**, 209.
38 R. Ugo, F. Cariati and G. La Monica, *Inorg. Synth.*, 1968, **11**, 105.
39 N. Walker and D. Stuart, DIFABS, *Acta Crystallogr.*, *Sect. A*, 1983, **39**, 158.
40 G. M. Sheldrick, SHELXTL, Version 5, *Software Reference Manual*, Siemens Industrial Automation Inc., Madison, WI, 1994.

Paper 8/09118H